JOURNAL OF GEOPHYSICAL RESEARCH, VOL. 104, NO. D10, PAGES 12,147–12,158, MAY 27, 1999

Microwave radiometric signatures of different surface types in deserts

Catherine Prigent [1]
Department of Applied Physics, Columbia University, NASA Goddard Institute for Space Studies, New York

William B. Rossow
NASA Goddard Institute for Space Studies, New York

Elaine Matthews
Center for Climate System Research, Columbia University, NASA Goddard Institute for Space Studies, New York

Béatrice Marticorena
Laboratoire Interuniversitaire des Systèmes Atmosphériques, Créteil, France

Abstract. In arid environments, specific microwave signatures have been observed with the Special Sensor Microwave /Imager (SSM/I). For a given diurnal change in surface skin temperature, the corresponding change in the microwave brightness temperature is smaller than expected. With the help of a one-dimensional, time-dependent heat conduction model, this behavior is explained by microwave radiation coming from different depths in the soil, depending on the soil type and on the microwave radiation frequency. Using the 8-times daily estimates of the surface skin temperature by the International Satellite Cloud Climatology Project (ISCCP) and a simple Fresnel model, collocated month-long time series of the SSM/I brightness temperatures and the surface skin temperatures give a consistent estimate of the effective microwave emissivity and penetration depth parameters. Results are presented and analyzed for the Sahara and the Arabian Peninsula, for July and November 1992. The case of the Australian desert is also briefly mentioned. Assuming a reasonable thermal diffusivity for the soil in desert areas, the microwave radiation is estimated to come from soil layers down to depths of at least five wavelengths in some locations. Regions where the microwave radiation comes from deeper soil layers also have large microwave emissivity polarization differences and large visible reflectances, suggesting that these areas correspond to sand dune fields. Two soil classification data sets show good correspondence of sand dunes and the microwave signature of significant penetration. This suggests that this analysis of microwave observations, along with other remote sensing technics, can be used to map the sand dunes in large, poorly surveyed deserts; a map of the sand dune fields in the Sahara and Saudi Arabia is derived from SSM/I observations.

1. Introduction

Passive microwave observations at frequencies below 10 GHz have been extensively studied for their potential to infer subsoil properties, especially soil moisture profiles (see *Wang and Choudhury* [1981], *Njoku and O'Neill* [1982], *Jackson and Schmugge* [1989], among others). A common approximation is that in bare soils the microwave radiation only emanates from a soil layer that is a wavelength or less thick because of strong extinction within the soil: The penetration depth, also referred to as the thermal sampling depth, is defined as the inverse of the extinction coefficient within the soil and is generally assumed to be of the order of a wavelength. As a consequence, frequencies over 15 GHz are not supposed to be suitable for the determination of any soil properties below the very first centimeter of

[1]On leave from Département de Radioastronomie Millimétrique, CNRS URA 336, Observatoire de Paris

Copyright 1999 by the American Geophysical Union.

Paper number 1999JD900153.
0148-0227/99/1999JD900153$09.00

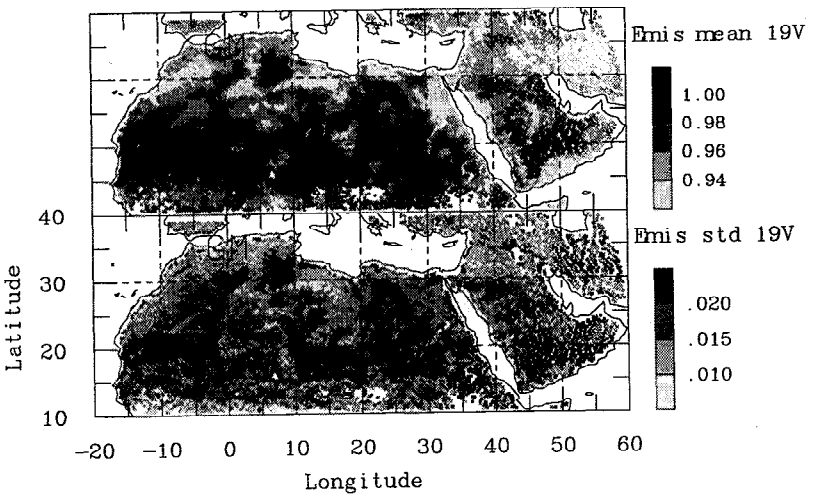

Figure 1. For July 1992, monthly mean emissivity at 19 GHz vertical polarization and the associated standard deviation over the month as calculated with the method described by *Prigent et al.* [1997].

the soil surface. The microwave emission at the surface is, in this case, proportional to the surface skin temperature, i.e., the temperature of the top first millimeter of the surface.

Microwave land surface emissivities over the globe have been estimated from the Special Sensor Microwave /Imager (SSM/I) observations at 19.35, 22.235, 37.0, and 85.5 GHz, by removing the contributions of the atmosphere, clouds, and rain using ancillary satellite data (International Satellite Cloud Climatology Project (ISCCP) and the National Centers for Numerical Prediction (NCEP)). See *Prigent et al.* [1997, 1998] for a description of the satellite data and the method. The retrievals are based on the assumption that the microwave radiation emanates only from a thin surface layer and that the surface temperature is thus the surface skin temperature estimated from infrared measurements. The standard deviation of day-to-day variations in the retrieved microwave emissivities within a month are typically about 0.012 for all the SSM/I frequencies, which is a measure of the accuracy of these estimates.

However, closer examination revealed that the standard deviations over specific arid areas are much higher (>0.02 at 19 GHz vertical polarization) than in surrounding areas (Figure 1). The estimated microwave surface emissivities in these areas at 19 GHz vertical polarization are also in some cases larger than 1 (Figure 1). A few possible causes have been examined without success. The possible variation of the SSM/I observations with azimuth angle has been explored. SSM/I always views the surface with a 53° incident angle, but, depending on the position of the pixel within a conical scan and depending on the satellite orbit (ascending or descending), a location on the Earth can be seen at different azimuth angles. Sorting the SSM/I observations into different azimuth angle ranges for each location does not reveal any differences, even in areas with strongly anisotropic slope orientations like in the Tenere Erg. Bias of the ISCCP estimates of the surface skin temperature by using unit IR emissivity in the retrieval might also cause these special microwave signatures. The accuracy of the surface skin temperature estimated by ISCCP has been thoroughly analyzed by *Rossow and Garder* [1993a, b]. The IR emissivity is mostly ≥0.95 but can be lower for bare, dry soils and rocks [*Salisbury and D'Aria*, 1992]. Overestimating the IR emissivities in these arid areas would be equivalent to a systematic underestimate of the temperature of at most 4 K, but a regional bias in the IR surface skin temperature is not sufficient to explain all of the observed microwave signatures.

In these desert environments, time series of IR surface temperatures and microwave brightness temperatures have been analyzed for July 1992, using the ISCCP surface skin temperatures and the SSM/I observations derived from the F11 and F10 Defense Meteorological Satellite Program (DMSP) satellites. In the arid areas associated with high emissivity standard deviations, these time series show that for a given magnitude diurnal change in surface temperature, the corresponding change in the microwave response is smaller in magnitude than expected and the discrepancy between the expected and observed changes increases with wavelength. Figure 2 compares the time series of microwave brightness temperatures and surface skin temperatures at two locations, one situated at 25°N and 12.5°E in an area of high emissivity standard deviations and a second location at 28°N and 17°E in an area where the emissivity standard deviation over a month is low.

Radar technics at longer wavelengths have been used to explore the surface and subsurface structures in arid areas. With the Shuttle Imaging Radar (SIR-A and SIR-B) operating at 1.25 GHz, subsurface valleys and geoarcheology have been revealed in the Eastern Sahara, thanks to a penetration depth of the radiation of 2 m and more below the surface [*McCauley et al.*, 1982; *Elachi et al.*, 1984]. More recently, the radars on ERS 1 at 5.3 GHz have also shown a good ability to charac-

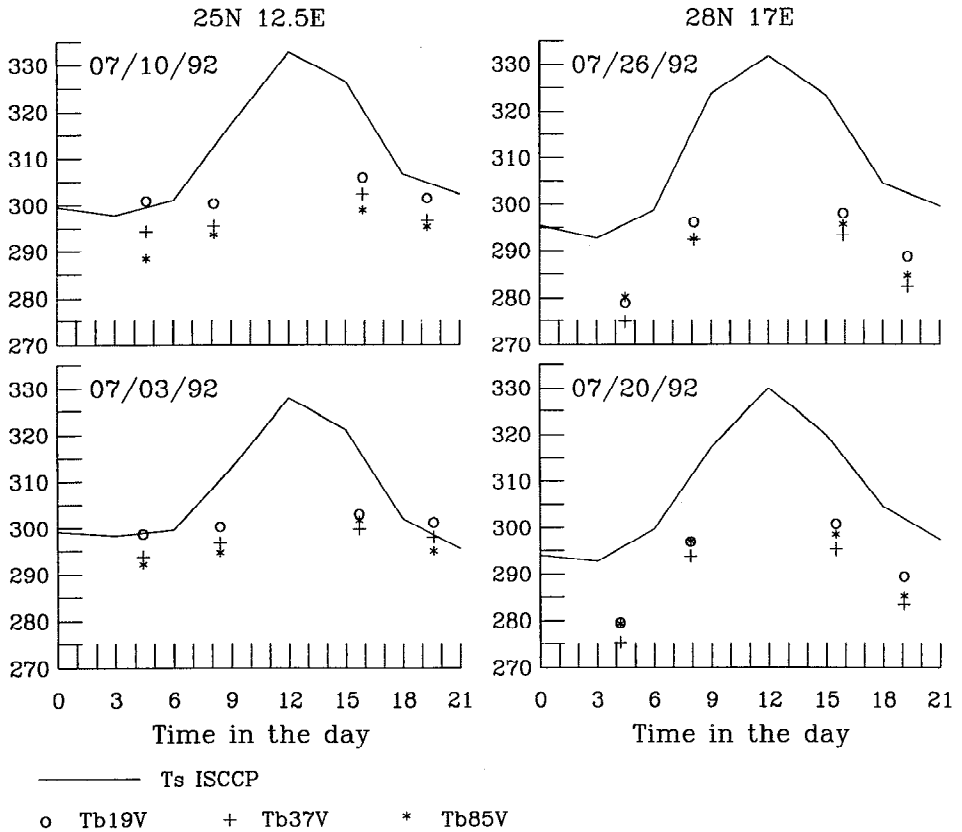

Figure 2. Time series of the SSM/I microwave brightness temperatures and the ISCCP surface skin temperature at two locations (25°N 12.5°E and 28°N 17°E) for different days in July 1992.

terize desert properties [*Deroin et al.*, 1997; *Frison and Mougin*, 1996].

Although SSM/I is operating at shorter wavelengths than these radars, we suggest that the observed behavior with SSM/I over the desert can be explained by microwave emissions from different layers in the soil, depending on the soil type and on the microwave radiation frequency. The soil subsurface temperature varies with time and depth such that with increasing depth in the soil, the amplitude of the diurnal temperature variation decreases and the phase lags as compared to the diurnal variation of the surface skin temperature. To examine our hypothesis, a one-dimensional, time-dependent heat conduction model is used to account for the transfer of heat in the soil over time and depth. On the basis of the 8-times daily estimates of the surface temperature from ISCCP, the diurnal cycle of the surface skin temperature is represented by the two first terms of a Fourier series fit. Then, using a simple Fresnel model for each individual location, the month-long time series of the seven SSM/I brightness temperatures and the surface temperature matchups are used to obtain best-fit estimates of the effective emissivity and a penetration depth parameter. Calculations are performed for the Sahara and the Arabian Peninsula, for July and November 1992, and for Australia, for July 1992. Correlation between the microwave properties of the surface and its visible reflectance is also examined. The results are interpreted in terms of soil material and texture with the help of soil-type classifications.

2. Methodology

2.1. Microwave Emission Model

All points within a soil emit microwave radiation depending on their temperature and absorptivity. From the point of origin to the soil surface, the radiation is attenuated by the intervening soil. The radiation emanating from the the soil surface is therefore a superposition of radiation emitted at various depths within the soil. For low microwave frequencies (below 10 GHz), Fresnel models have been widely used in the literature to describe the microwave response to the subsoil temperature changes, along with an effective temperature and an effective emissivity [*Choudhury et al.*, 1982; *Schmugge and Choudhury*, 1981; *Raju et al.*, 1995; *Chanzy et al.*, 1997]. The Fresnel model assumes that the soil can be described by a single layer at a depth d_{eff} associated with a given effective temperature T_{eff} from which all the radiation will emanate. Reflection can only take place at the air-soil interface and the model ignores all reflections within the soil medium. The air-soil interface is characterized by an effective emissivity ϵ_{eff}. With this assumption, the radiative transfer equation can be expressed in terms of brightness temperature for each orthogonal polarization p (p stands

for either horizontal, $_H$, or vertical, $_V$):

$$Tb_P = T_{eff}\epsilon_{eff P}e^{-\tau(0,H)\sec\theta} + T_a\downarrow(1-\epsilon_{eff P})e^{-\tau(0,H)\sec\theta} + T_a\uparrow \quad (1)$$

with $T_a\downarrow = \int_0^H T(z)\alpha(z)\sec\theta e^{-\tau(0,z)\sec\theta}dz$ and $T_a\uparrow = \int_0^H T(z)\alpha(z)\sec\theta e^{-\tau(z,H)\sec\theta}dz$.
Tb_P is the brightness temperature measured by the satellite for polarization $_P$; θ is the incident angle at the surface, i.e., 53° for the SSM/I observations; $\alpha(z)$ is the atmospheric absorption by gases at altitude z; $T(z)$ is the atmospheric temperature at altitude z; $\tau(z_0, z_1) = \int_{z_0}^{z_1}\alpha(z)dz$ is the atmospheric opacity from z_0 to z_1; and H is the satellite altitude.

The use of the Fresnel model usually requires knowledge of several soil characteristics (Fresnel reflection coefficients, subsoil temperature profile). In this study, we propose to derive the subsoil temperature profile from a simple one-dimensional, time-dependent heat conduction model to account for the depth and time transfer of heat in the soil and to use the ISCCP surface skin temperature time series to obtain the surface boundary conditions. Then, for each location, the T_{eff} (at a depth d_{eff} below the soil surface) and the ϵ_{eff} at each wavelength are estimated to minimize the root mean square error between the month-long time series of the measured Tb and the Tb simulated by equation (1) at that location.

2.2. One-Dimensional Time-Dependent Heat Conduction Model

The equation that governs the time and depth variation of the temperature when heat is transfered in one dimension by conduction is given by the Fourier heat conduction law:

$$k\frac{\partial^2 T(d,t)}{\partial d^2} = \rho c\frac{\partial T(d,t)}{\partial t} \quad (2)$$

with $T(d,t)$ being the temperature at a depth d and time t; k is the thermal conductivity; c is the specific heat capacity, and ρ is the soil density. Equation (2) is like a diffusion equation and can be rewritten in terms of $\kappa = k/(\rho c)$, called the thermal diffusivity. As stated, equation (2) assumes that the heat is transfered in one dimension only. It also supposes that the soil properties (thermal conductivity, specific heat capacity, and density) are constant with depth and are homogeneous within the 30 km pixels we are considering. These simple assumptions may not be strictly valid in each location, but the lack of available information on these parameters for large geographic areas precludes more refined treatment of the physics involved.

The daily cycle of solar heating and cooling is the driving flux at the soil surface with a period of 24 hours and an angular frequency $\omega_0 = 2\pi/(3600\times 24)$ rad/s. At a depth d from the Earth's surface, $T(d,t)$ oscillates with the fundamental period of 24 hours plus various harmonics of that fundamental frequency. The amplitude of the oscillation decays with depth, and the phase difference between the oscillation at the surface and at depth d increases with d. Writing a solution for $T(d,t)$ purely in terms of real quantities means using a solution of the form

$$T(d,t) = T_0 + \sum_n A_n exp(-d\sqrt{\frac{n\omega_0}{2\kappa}})\cos(n\omega_0 t + \phi_n - d\sqrt{\frac{n\omega_0}{2\kappa}}) \quad (3)$$

At the surface, this equation reduces to

$$T(0,t) = T_0 + \sum_n A_n\cos(n\omega_0 t + \phi_n). \quad (4)$$

The coefficients T_0, A_n, and ϕ_n are calculated to fit the boundary conditions at the surface of the Earth, determined for each location by the 8-times daily ISCCP estimates of the surface skin temperature. The spatial resolution of the ISCCP DX product is ~30×30 km^2 (see *Rossow et al.* [1996] for a detailed description of the ISCCP products and for further references). The Fourier series is limited to its first two terms which provides adequate accuracy. Figure 3 presents an example of the diurnal cycle of surface skin temperatures and the fit obtained from a two-term Fourier series fit. Also shown are the diurnal cycles of the temperature at two different depths for a thermal diffusivity of 0.002 cm^2/s, typical of dry quartz sand [*Ingersoll et al.*, 1948]. The rms error of the fit is 1.37 K for July 1992 for the studied area (the Sahara and the Arabian Peninsula). South of 15°N, the rms error of the fit is slightly larger because the maximum amplitude of the diurnal temperature oscillation can be small in this area (~ 5 K), i.e., rather

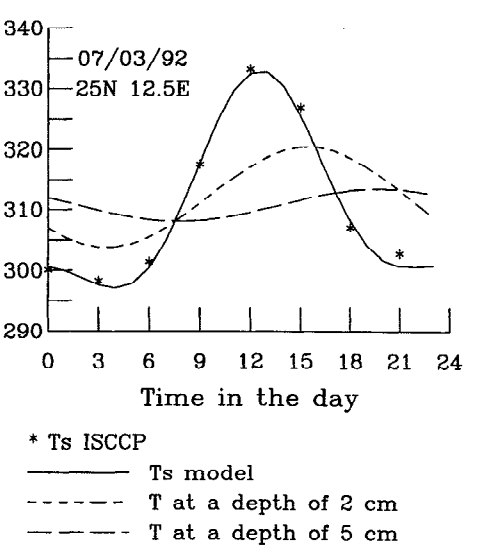

Figure 3. Diurnal cycle of the surface skin temperature at 25°N 12.5°E July 3, 1992, along with the fit obtained from a two term expansion of the Fourier equation at the surface, at 2 cm below the soil surface, and at 5 cm below the soil surface.

close to the accuracy of the IR estimate of the surface temperature itself.

2.3. Effective Temperature and Emissivity

For each 30×30 km^2 location, the times series of the SSM/I observations have been collected for two DMSP satellites that are in orbit simultaneously. Pixels characterized as cloudy by the ISCCP procedure are not considered (for a description of the cloud-clearing procedure, see *Prigent et al.* [1997]).

Equations (1) and (3) are combined to give

$$Tb_P = [T_0 + \sum_{n=1,2} A_n exp(-d_{eff}\sqrt{\frac{n\omega_0}{2\kappa}})$$
$$\cos(n\omega_0 l + \phi_n - d_{eff}\sqrt{\frac{n\omega_0}{2\kappa}})]\epsilon_{effP} e^{-\tau(0,H)\sec\theta} +$$
$$T_a \downarrow (1-\epsilon_{effP})e^{-\tau(0,H)\sec\theta} + T_a \uparrow \qquad (5)$$

for a measurement at time t over a surface with an effective emissivity ϵ_{eff}, for a thermal diffusivity κ, and assuming that the effective temperature T_{eff} of the sounded soil layer corresponds to the soil temperature at depth d_{eff}. Coefficients T_0, A_n, and ϕ_n have been calculated for each location as described above. Equation (5) implies that both the amplitude and the phase of the signal vary with the sounding depth d_{eff}. For each SSM/I frequency, the atmospheric contributions τ, $T_a \downarrow$, and $T_a \uparrow$ are estimated from the temporally and spatially coincident atmospheric profiles given by NCEP every 2.5° × 2.5° and every 6 hours (as described by *Prigent et al.* [1998]). A nonlinear least squares method is used to estimate the ϵ_{eff} and the $(d_{eff}\sqrt{\omega_0/2\kappa})$ that will minimize the difference between the Tb simulated by equation (5) and the measured Tb over a month. The results are given in terms of the effective emissivity ϵ_{eff} and the unitless parameter

$$\alpha = d_{eff}\sqrt{\omega_0/2\kappa} \qquad (6)$$

3. Results and Correlation With Other Surface Properties

The F10 and F11 SSM/I data have been processed for July 1992, for the Sahara and for the Arabian Peninsula. Maps of the estimated ϵ_{eff} are presented at 19, 37, and 85 GHz for both vertical and horizontal polarizations, along with the corresponding maps of the α parameter (Plate 1). Figure 4a presents the difference between the monthly mean emissivity estimated with the method described by *Prigent et al.* [1997] and the effective emissivity ϵ_{eff} at 19 GHz (vertical polarization) estimated in this study as a function of α for the same channel. The difference is significant only for areas where α is large (92% of pixels with difference $\geq$ 0.01 correspond to $\alpha \geq$ 0.5). When more of the microwave radiation comes from greater depths in the soil, the difference between T_{eff} and the temperature at the surface T_s is larger and as a consequence, the difference between the emissivity calculated using T_s and the

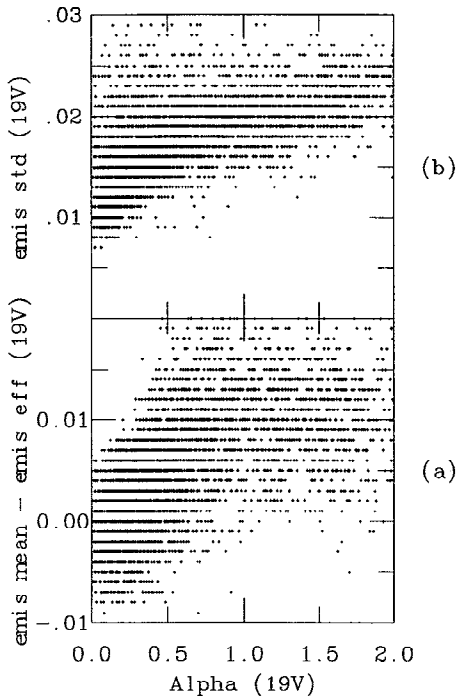

Figure 4. At 19 GHz vertical polarization, (a) difference between the monthly mean emissivities previously calculated [*Prigent et al.*, 1997] and ϵ_{eff} now estimated versus α and (b) standard deviation of the emissivity previously calculated over a month versus α.

emissivity calculated using T_{eff} is also larger. Figure 4b shows that large values of α also correspond closely to the areas where the standard deviation of day-to-day variations of the emissivity as calculated over a month was large (80% of pixels with standard deviations $\geq$ 0.02 correspond to $\alpha \geq$ 0.5).

Converting α to a penetration depth d_{eff} is not straightforward because survey maps of the thermal diffusivity κ are not available. Very few measurements of this parameter are reported in the literature, but a mean value of 0.004 cm^2/s for the globe has been proposed with a value of 0.002 cm^2/s for dry quartz sand [*Ingersoll et al.*, 1948; *Lettau*, 1951; *Sellers*, 1965]. From equation (6), α increases with decreasing κ. Assuming a value of 0.002 cm^2/s for κ in these arid areas, α is multiplied by 7.4 to derive the penetration depth d_{eff} in cm. At 19 GHz vertical polarization, areas with α over 1.2 have a penetration depth d_{eff} larger than 8 cm, i.e., larger than five wavelengths. For κ=0.004 cm^2/s, α is multiplied by 10.5 to give d_{eff}, but this value of κ is probably not realistic for dry sand. Although the penetration depth in a soil is commonly assumed to be of the order of a wavelength or less, a few studies have shown that in very dry sands, the penetration depth of microwave radiation can be much larger. *Campbell and Ulrichs* [1969] measured penetration depths at 35 GHz between 5 and 50 wavelengths in powdered rocks. Recently, *Matzler* [1998] measured the dielectric properties of dry desert sand between 1 and 10 GHz and concluded that the penetration depth in this frequency

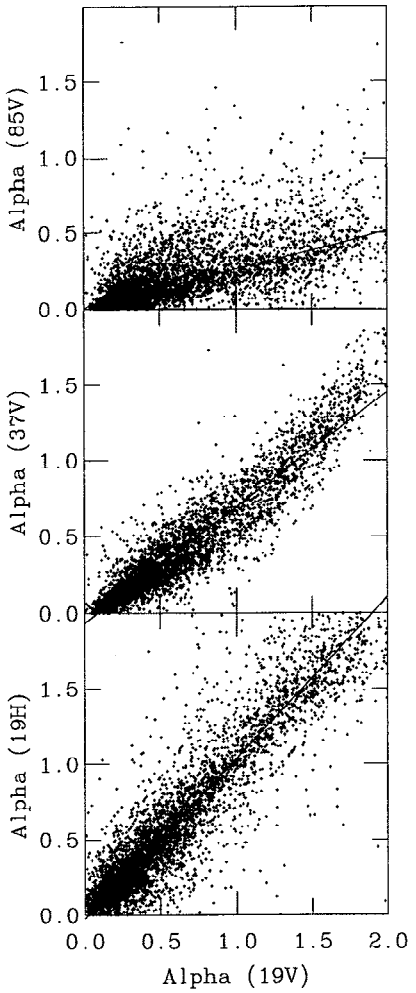

Figure 5. Scatterplots of α at 19 GHz vertical polarization versus its values at 19 GHz horizontal polarization and at 37 and 85 GHz for vertical polarization.

range is around 1 m with only a small decline with increasing frequency. When soil moisture increases, the penetration depth sharply decreases [*Njoku and O'Neill*, 1982], and areas of high α are necessarily very dry.

The scatterplots in Figure 5 show the relationship between α at 19 GHz vertical polarization and α at 19 GHz horizontal polarization, and at 37 and 85 GHz vertical polarization. The α values at horizontal and vertical polarizations for a given frequency are similar (results are not presented at 37 and 85 GHz). As expected, α decreases with increasing frequencies: The lower the frequency, the deeper the penetration into the soil. The ratio between α at 19 and 37 GHz (respectively at 85 GHz), given by the slope of the linear regression, is higher than the wavelength ratio: 0.76 for the slope of the regression between 19 and 37 GHz as compared to 0.51 for the ratio of wavelengths (respectively 0.26 compared to 0.22 between 19 and 85 GHz). This feature tends to follow Matzler's results, that the frequency dependence of the penetration depth is weaker than expected.

The zonal mean standard deviations of the theoretical errors for the two retrieved parameters are calculated from the fit. For latitudes above 20°N, the errors are lower than 0.003 and 0.1 for ϵ_{eff} and α, respectively. The error increase at lower latitudes is explained by the larger relative error in the estimates of the diurnal temperature cycle at the surface.

To estimate the surface temperature, the ISCCP procedure assumes that the IR emissivity is 1, but the IR emissivity can be lower (≤ 0.95) for bare and dry soils [*Salisbury and D'Aria*, 1992]. Overestimating the emissivity in these areas is equivalent to an underestimate of the IR surface temperature by at most 4 K. Examination of equations (4) and (5) shows that an underestimate of the surface temperature of this magnitude affects only the estimated ϵ_{eff} (an overestimate of $\sim$ 0.014, i.e., close to 4 K/300 K) and does not have a significant impact on the estimate of α. This has been confirmed by sensitivity tests.

The interpretation of these results is based on an analysis of the correlations between the geographical patterns of the microwave signatures and the spatial variations of other surface properties. We examine maps of the surface visible ((VIS) $\sim$0.6μm wavelength) reflectance and available soil classifications.

3.1. Correlation With the VIS Reflectance

The mean surface VIS reflectance (as a proxy of albedo) estimated by ISCCP from the Meteosat satellite is presented in Figure 6 for July 1992. The estimated VIS reflectances have been averaged over the month, ignoring angular variations. The mean surface reflectance shows rather large variations over the desert from values as low as 0.15 in the mountainous area of the Tibesti

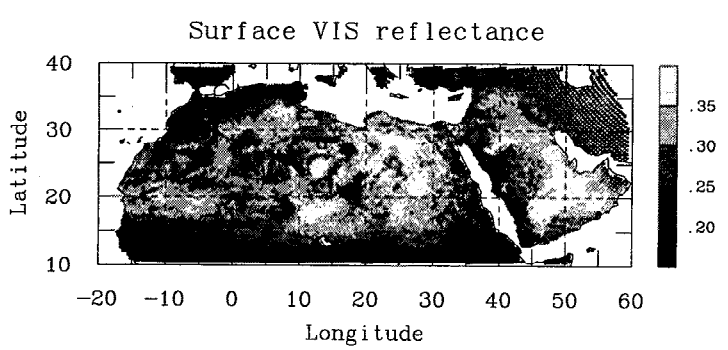

Figure 6. ISCCP estimation of the VIS reflectance in the studied area for July 1992.

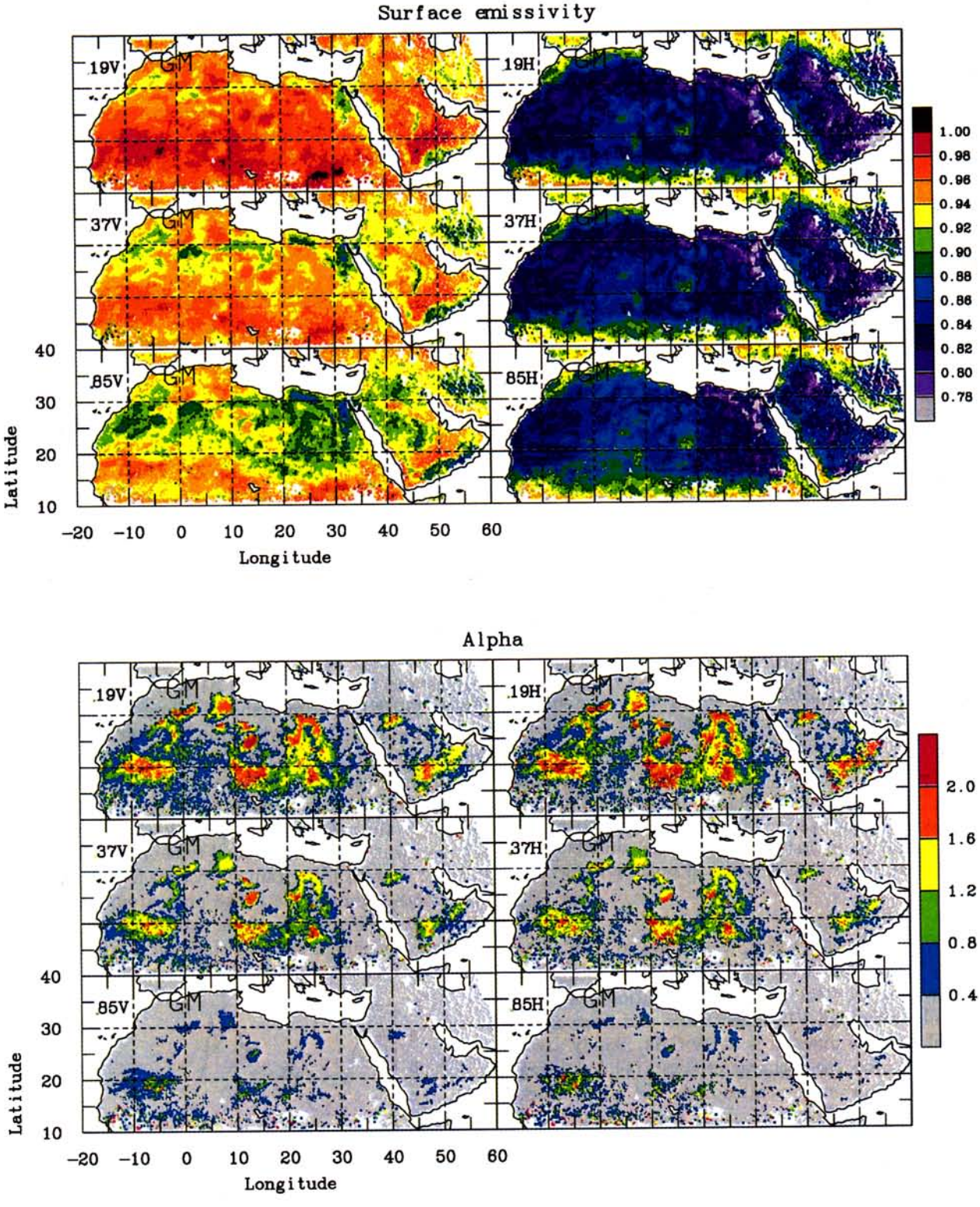

Plate 1. Maps of the estimated ϵ_{eff} at 19, 37, 85 GHz for vertical and horizontal polarizations and the corresponding maps of the α parameter.

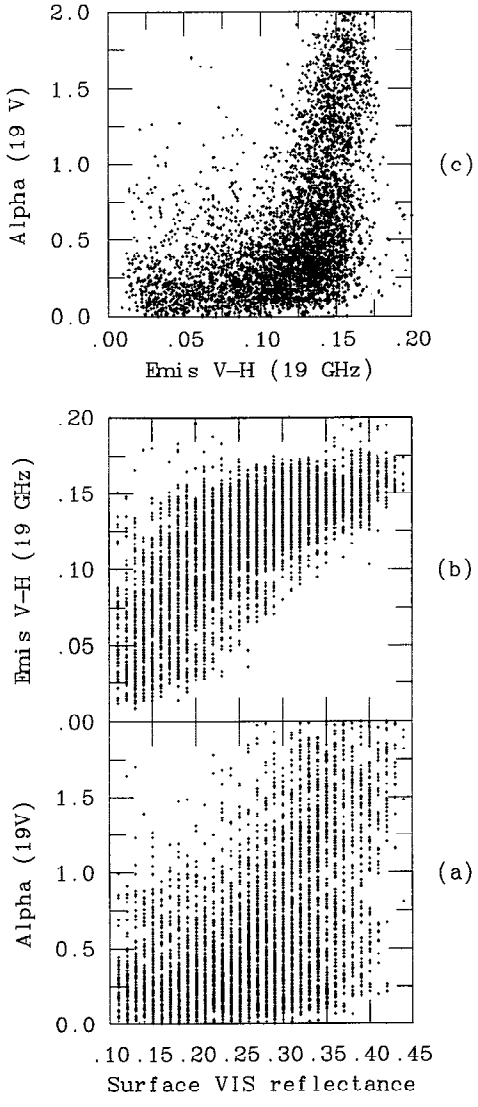

Figure 7. Scatterplots of the VIS reflectance versus (a) α at 19 GHz vertical polarization and (b) versus the emissivity polarization difference at 19 GHz; (c) scatterplot of the emissivity polarization difference at 19 GHz versus α at 19 GHz vertical polarization.

(around 20°N and 18°E) up to values over 0.40 in some places in Libya and Egypt. Figure 7 shows that large values of α at 19 GHz vertical polarization are associated only with high VIS reflectances and large emissivity polarization differences at 19 GHz. Sandy areas are likely to have these characteristics: (1) scattering by quartz sand grains generates high VIS reflectances; (2) in dry places, a large emissivity polarization difference can be caused by surfaces with a quasi-specular behavior; (3) in dry sand, α can be large because the penetration depth is larger in the absence of moisture and because the thermal diffusivity is much smaller in dry quartz sand than in other materials [*Ingersoll et al.*, 1948].

3.2. Correlations With Physical Soil Properties

Detailed descriptions of the surface soil characteristics in desert areas are not easily found. The Food and Agriculture Organization of the United Nation Educational, Scientific and Cultural Organization (FAO-UNESCO) has produced a 1:5,000,000 soil map of the world [*FAO-UNESCO*, 1977], based on in situ surveys. The dominant soils are provided, along with macro-structure differences (presence of rocks, pebbles, sand on the soil). The information concerning the dominant soils has been digitized with a 1° × 1° resolution by *Zobler* [1986], but the soil macro-structure properties are not provided in this file. A visual examination of the original FAO-UNESCO soil map shows good similarity between the areas characterized as sand dunes by the FAO-UNESCO classifications and the areas of large α at 19 GHz. To better quantify the correlation between these characteristics, the sand dunes areas have been digitalized with a 1° × 1° resolution, and the result is presented in Plate 2a. The underlying soil type is indicated when that information is available. Plate 2b illustrates the correspondence between the presence of sand and the values of α at 19 GHz vertical polarization. Except for the yermosols and lithosols, sand dunes and shifting sand are mostly associated with large values of α at 19 GHz. Characterization of yermosols is very vague in the FAO-UNESCO classification and is related to the moisture regime at the surface; the fact that this type of surface is not associated with large α is difficult to interpret. Lithosols consist of hard rocks with less than 10 cm soil cover and, because penetration depth is smaller in solid rocks than in the corresponding powder rock (of the order of 5 times smaller [*Campbell and Ulrichs*, 1969]), α is expected to be much smaller for this type of soil. The size of the FAO sand dune regions and the regions of $\alpha \geq 1$ at 19 GHz can differ. The FAO-UNESCO map shows a large sand dune field around 25°N and 2°W, while α in this area is mostly <1. On the contrary, around 22°N and 22°E, α is above 1 although the sand dune areas are smaller (several small areas of sand dunes are observed on the 1:5,000,000 soil maps but are not shown in Plate 2a because they do not represent the dominant soil type on a 1° × 1° grid). Figure 8 shows a histogram of α values for all FAO sand dune areas, exhibiting a broad peak around a value of 1.6, while the histogram of the pixels that are not classified as sand dunes shows a single peak at very low α

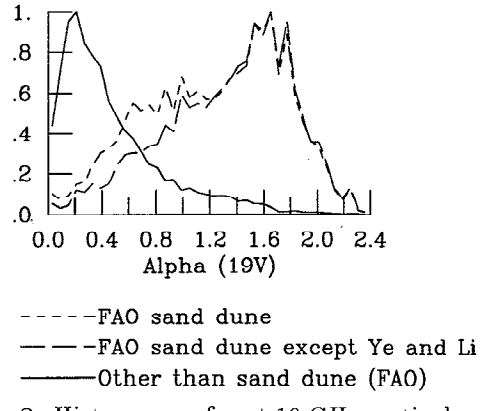

Figure 8. Histograms of α at 19 GHz vertical polarization for the sand dunes and shifting sands as classified by FAO-UNESCO.

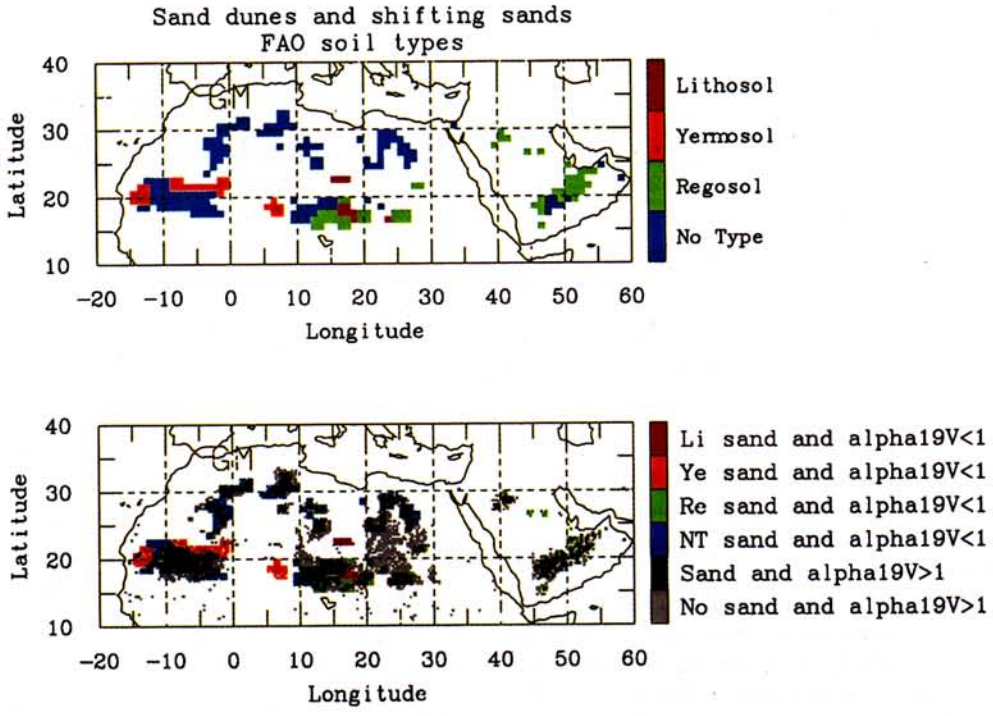

Plate 2. (a) The sand dune and shifting sand types by FAO-UNESCO; (b) correspondence between the FAO-UNESCO sand dunes and α at 19 GHz vertical polarization.

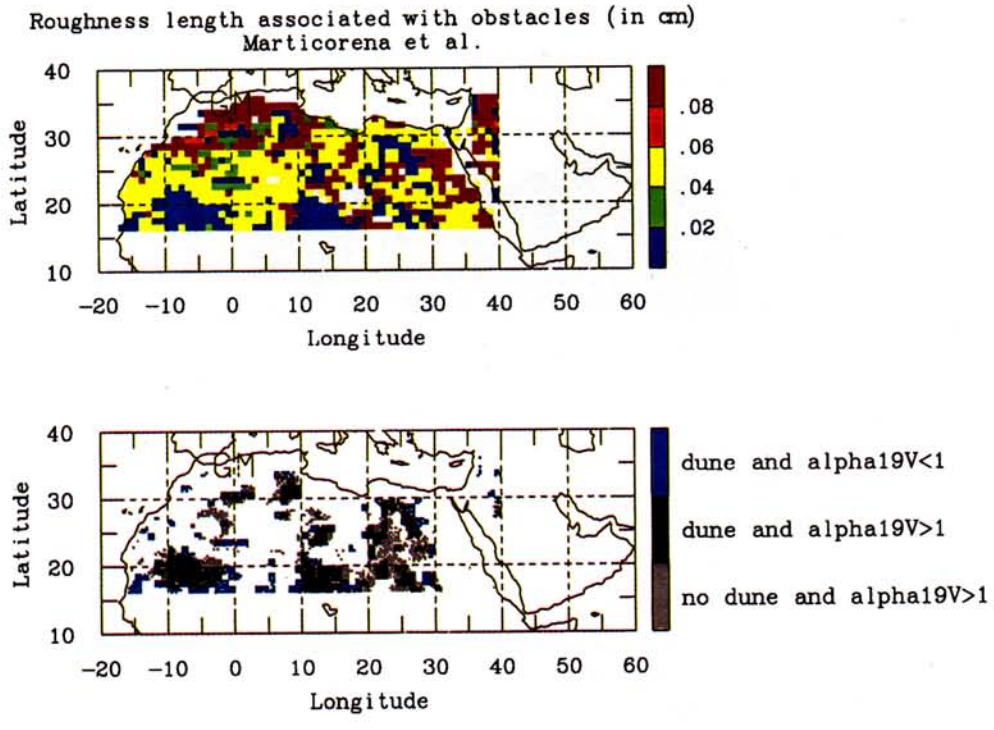

Plate 3. (a) Classification of the sand dunes by *Marticorena et al.* [1997]; (b) correspondences between the sand dunes as classified by *Marticorena et al.* [1997] and α at 19 GHz vertical polarization.

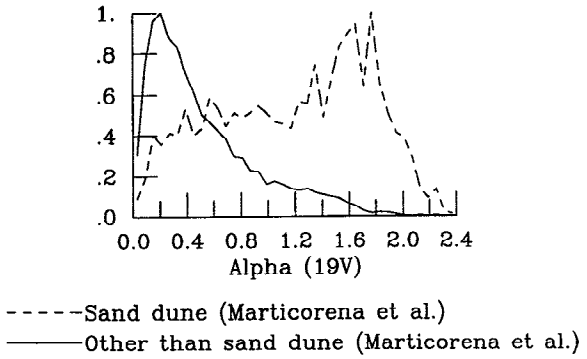

Figure 9. Histograms of α at 19 GHz vertical polarization for the sand dunes as classified by *Marticorena et al.* [1997].

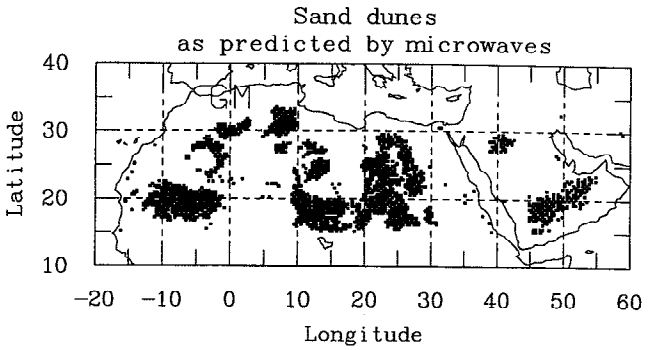

Figure 10. Maps of the sand dune fields for the Sahara and the Arabian Peninsula as estimated from microwave.

values. The large tail of the histogram at lower α values for FAO sand dune areas can represent pixels which are only partly covered by sand dunes or pixels covered by a thinner layer of sand.

A second classification of desert soil properties, mainly derived from the examination of topographical maps, has also been used to help interpret the microwave signature. This detailed classification is described by *Marticorena et al.* [1997] and covers up to 40°E and down to 16°N. Each one square degree grid mesh is characterized by up to five surface feature types, giving their surface cover fraction within the grid. Each of the five surface features is then characterized by its dominant mineralogical soil type, the roughness length of the bare soil, the roughness length of potential obstacles on the surface (pebbles, rocks, gravels), and the fraction of the surface the obstacles cover.

Coarse and fine sands often coexist in the same areas and generally correspond to dune fields [*Marticorena et al.*, 1997]. These areas are generally free of obstacles and have a low roughness length. Plate 3a represents the roughness length associated with obstacles as estimated by Marticorena et al. Roughness lengths that are below 0.02 cm generally characterize sand dunes, so this threshold can be used to map sand dunes. Areas characterized as sand dunes or shifting sands in the FAO-UNESCO classification correspond in 60% of the cases to roughness lengths below 0.02 cm. The main differences lie in the size of the dune fields, but sand dunes shown in one classification are absent in the other. The large dune field around 2.5°W and 27°N in the FAO

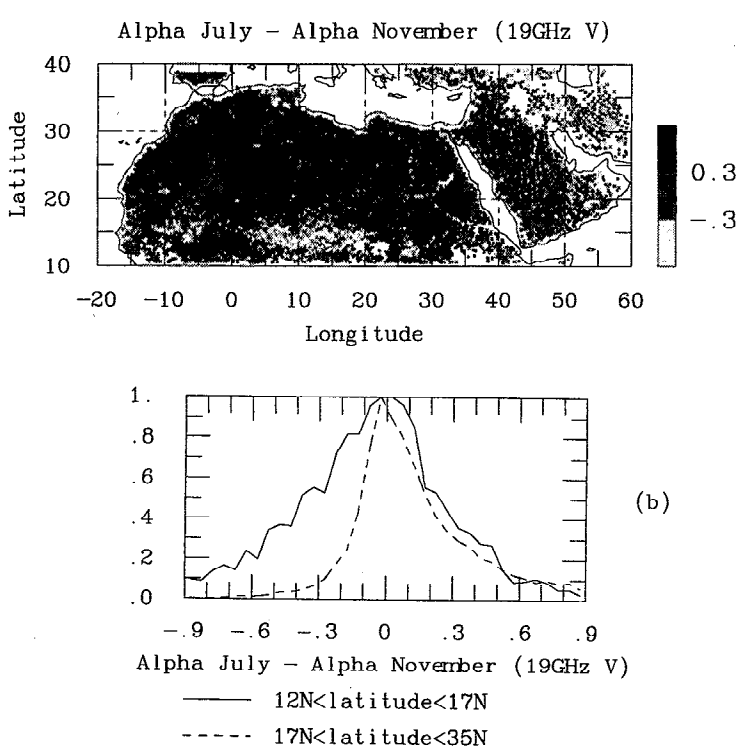

Figure 11. (a) Map of the difference of α between July 1992 and November 1992 for 19 GHz vertical polarization; (b) histograms of the difference for two latitude ranges.

classification does not correspond to dunes in Marticorena et al.'s classification. The sand dune around 20°N and 8°W is larger southward in Marticorena et al.'s classification than in the FAO one. Plate 3b shows the correlation between sand dunes as characterized by Marticorena et al.'s classification and the α=1 threshold at 19 GHz vertical polarization. The histogram of the sand dune population in Figure 9 again shows a peak for α 19 GHz vertical polarization around 1.6, while the histogram is centered around a very low value of α for areas that are not characterized as sand dunes.

Comparisons of the microwave signatures with the two soil data sets show that α at 19 GHz vertical polarization could be used to map the sand dune fields in the deserts. The paucity of available field data in these arid regions makes the satellite observations a very attractive tool to study these environments. When applying a threshold α=1 at 19 GHz vertical polarization and suppressing the pixels associated with large errors in the determination of this parameter (i.e., pixels located below 15°N and on the coasts), a map of the sand dune fields is obtained for the Sahara and the Arabian Peninsula (Figure 10).

To illustrate the stability of this result, we repeat the analysis for November 1992 and show the difference of α between July and November at 19 GHz vertical polarization (Figure 11). For latitudes below 17°N, a significant number of pixels are characterized by larger α in November than in July. This is consistent with increased soil moisture near the northern limit of the Inter Tropical Convergence Zone going southward from summer to winter. For latitudes above 17°N, the sand dune areas show slightly smaller values of α in November than in July. Larger α values in July are also consistent with dryer soils than in November that provide larger dust sources: In the Sahara, dust emissions are at their lowest values at the beginning of the winter [*Marticorena et al.*, 1997].

The same methodology has been applied to Australia for July 1992 using the ISCCP data derived from the Geostationary Meteorological Satellite. Maps of the emissivity polarization difference and α at 19 GHz are presented along with the VIS reflectance (Figure 12). The areas where the microwave radiation comes from deeper in the soil (α higher than one) are mostly limited to the Great Sandy Desert in the north-west which is characterized by a shallow sandy soil. The Australian deserts are much darker than the African deserts, with VIS reflectances generally below 0.2. Although associated to high VIS reflectance, the Simpson desert in the center of the country does not exhibit large α values.

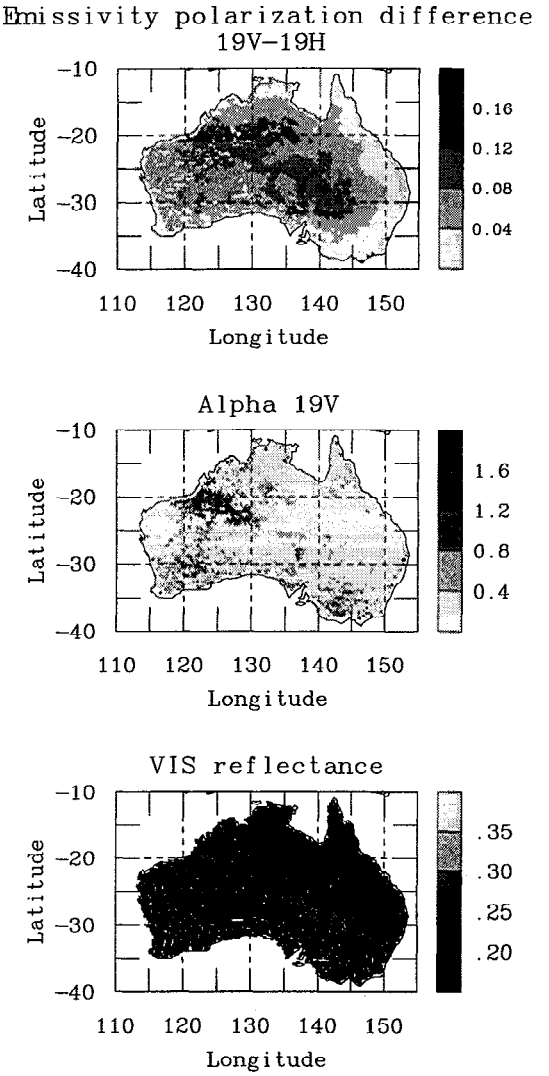

Figure 12. Maps of the emissivity polarization difference at 19 GHz and α at 19 GHz vertical polarization for Australia for July 1992. ISCCP estimations of the VIS reflectances are also shown for the same month.

4. Conclusion

In arid environments, specific microwave signatures have been observed. They can be explained by emissions of microwave radiations from different layers in the subsoil, depending on the soil type and on the microwave radiation frequency. Results are presented and analyzed in detail for the Sahara and the Arabian Peninsula. The case of the Australian desert is briefly discussed. Assuming a thermal diffusivity of the soil of 0.002cm^2/s, the penetration depth of microwave is estimated to be larger than five wavelengths in some locations, indicating extremely dry conditions. Regions where the microwave radiation comes from deeper in the soil correspond to regions of large emissivity polarization differences and large VIS reflectances, suggesting that these areas correspond to sand dune fields. Two soil classifications have been examined to help interpret the microwave signatures. Comparison of the microwave signatures with these soil data sets shows that the parameter α at 19 GHz vertical polarization can be used to map sand dune areas in the deserts. A map of the sand dune fields is then presented derived from the microwave observations. Given the scarcity of measurements of soil properties in arid environments, remote sensing technics are particularly attractive. Radar ob-

servations (see for instance *McCauley et al.* [1982] and *Deroin et al.* [1997]) have already been used to study desert characteristics, and passive and active microwave observations should be jointly analyzed in the future to investigate their complementarity. Deserts occupy~ 12% of the global ice-free land surface and present a large variety of soil and rock material. An improved understanding of the arid environments could help better determine natural mineral aerosol sources, which are primary inputs to model the atmospheric dust cycle.

Acknowledgment. This work is supported by NASA Mission to Planet Earth program. We would like to thank Yann Callot (Tours University, France) for fruitful discussions on desert characteristics. We are grateful to Jean-Pierre Wigneron (INRA, Avignon, France) and Yann Kerr (CESBIO, Toulouse, France) for their comments on the manuscript. We also thank Dr. Schmugge and two other anonymous reviewers for their careful reading of the manuscript and for valuable suggestions. NCAR/NCEP Reanalysis data have been provided through the NOAA Climate Diagnostics center (http://www.cdc.noaa.gov).

References

Campbell, M. J., and J. Ulrichs, Electrical properties of rocks and their significance for lunar radar observations, *J. Geophys. Res.*, *74*, 5867-5881, 1969.

Chanzy, A., S. Raju, and J.-P. Wigneron, Estimation of soil microwave effective temperature at L and C bands, *IEEE Trans. Geosc. Remote Sens.*, *35*, 570-579, 1997.

Choudhury, B. J., T. J. Schmugge, and T. Mo, A parameterization of effective soil temperature for microwave emission, *J. Geophys. Res.*, *87*, 1301-1304, 1982.

Deroin, J. P., A. Company, and A. Simonin, An empirical model for interpreting the relationship between backscattering and arid land surface roughness as seen with SAR, *IEEE Trans. Geosc. Remote Sens.*, *35*, 86-92, 1997.

Elachi, C., L. E. Roth, and G. G. Schaber, Spaceborne radar subsurface imaging in hyperarid regions, *IEEE Trans. Geosc. Remote Sens.*, *22*, 383-387, 1984.

Food and Agriculture Organization of the United Nations - United Nations Educational, Scientific and Cultural Organization, Soil map of the world, scale 1:5M , UNESCO, Paris, 1977.

Frison, P. L., and E. Mougin, Use of ERS-1 wind scatterometer data over land surface, *IEEE Trans. Geosc. Remote Sens.*, *34*, 550-560, 1996.

Ingersoll, L., O. J. Zobel, and A. C. Ingersoll, *Heat Conduction*, McGraw-Hill, New York, 1948.

Jackson, T. J., and T. J. Schmugge, Passive microwave remote sensing system for soil moisture: Some supporting research, *IEEE Trans. Geosc. Remote Sens.*, *27*, 225-235, 1989.

Lettau, H., Theory of surface-temperature and heat-transfer oscillation near a level ground surface, *Eos Trans. AGU*, *23*, 189-200, 1951.

Marticorena, B., G. Bergametti, B. Aumont, Y. Callot, C. N'Doumi, and M. Legrand, Modeling the atmospheric dust cycle, 2, Simulation of Saharan dust sources, *J. Geophys. Res.*, *102*, 4387-4404, 1997.

Matzler, C., Microwave permittivity of dry sand, *IEEE Trans. Geosc. Remote Sens.*, *36*, 317-319, 1998.

McCauley, J. F., G. G. Schaber, C. S. Breed, M. J. Grolier, C. V. Haynes, B. Issawi, C. Elachi, and R. Bloom, Subsurface valleys and geoarcheology of eastern Sahara revealed by shuttle radar, *Science*, *218*, 1004-1019, 1982.

Njoku, E. G., and P. E. O'Neill, Multifrequency microwave radiometer measurements of soil moisture, *IEEE Trans. Geosc. Remote Sens.*, *20*, 468-475, 1982.

Prigent, C., W. B. Rossow, and E. Matthews, Microwave land surface emissivities estimated from SSM/I observations, *J. Geophys. Res.*, *102*, 21867-21890, 1997.

Prigent, C., W. B. Rossow, and E. Matthews, Global maps of microwave land surface emissivities: Potential for land surface characterization, *Radio Sci.*, *33*, 745-751, 1998.

Raju, S. A., Chanzy, J.-P. Wigneron, J.-C. Calvet, Y. Kerr, and L. Laguerre, Soil moisture and temperature profile effects on microwave emission at low frequencies, *Remote Sens. Environ.*, *54*, 85-97, 1995.

Rossow, W. B., and L. C. Garder, Cloud detection using satellite measurements of infrared and visible radiances for ISCCP, *J. Clim.*, *6*, 2341-2369, 1993a.

Rossow, W. B., and L. C. Garder, Validation of ISCCP cloud detections, *J. Clim.*, *6*, 2370-2393, 1993b.

Rossow, W. B., A. W. Walker, D. E. Beuschel, and M. D. Roiter, International Satellite Cloud Climatology Project (ISCCP): Document on new cloud datasets, NASA Goddard Inst. for Space Stud., New York, 1996.

Salisbury, J. W., and D. M. D'Aria, Emissivity of terrestrial materials in the 8-14μm atmospheric window, *Remote Sens. Environ.*, *42*, 83-106, 1992.

Schmugge, T. J., and B. J. Choudhury, A comparison of radiative transfer models for predicting the microwave emission from soils, *Radio Sci.*, *16*, 927-938, 1981.

Sellers, W. A., Physical Climatology, Univ. of Chicago Press, Chicago, Ill., 1965.

Wang, J. R., and B. J. Choudhury, Remote sensing of soil moisture content over bare field at 1.4 GHz frequency, *J. Geophys. Res.*, 86, 5277-5282, 1981.

Zobler, L., A world file for global climate modeling, *Tech. Rep.*, *NASA-TM-87802*, NASA, 1986.

B. Marticorena, Laboratoire Interuniversitaire des Systèmes Atmosphériques, URA CNRS 1404, Centre Multidisciplinaire de Créteil, 61, Avenue du Général de Gaulle, 94 010 Créteil, France

E. Matthews, Center for Climate System Research, Columbia University, NASA Goddard Institute for Space Studies, 2880 Broadway, New York, N.Y. 10025.

C. Prigent,Department of Applied Physics, Columbia University, NASA Goddard Institute for Space Studies, 2880 Broadway, New York, N.Y. 10025. e-mail: cprigent@giss.nasa.gov

W. B. Rossow, NASA Goddard Institute for Space Studies, 2880 Broadway, New York, N.Y. 10025

(Received August 24, 1998; revised December 17, 1998; accepted February 25, 1999.)